A comparison between LQG and MPC autopilots for inclusion in a navigation, guidance and control system

A SK Annamalai, A Motwani

School of Marine Science and Engineering
Plymouth University, Plymouth

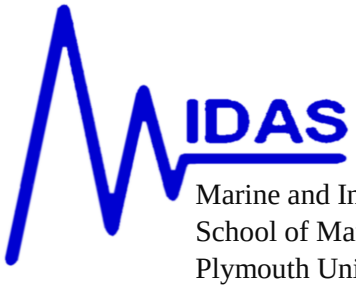

Marine and Industrial Dynamic Analysis
School of Marine Science and Engineering
Plymouth University, PL4 8AA

TECHNICAL REPORT

1 March 2013

MIDAS.SMSE.2013.TR.006

Abstract

Integrated navigation, guidance and control systems are designed for an uninhabited surface vehicle named *Springer* built at Plymouth University. Kalman filtering is used for navigation and line of sight is used for guidance. Linear quadratic Gaussian and model predictive control are utilised to build the control system for the autopilots. The performance of these two autopilots in conjunction with the navigation and guidance subsystems are compared and analysed in this technical report.

KEY WORDS

1. Navigation, guidance and control. 2. Uninhabited surface vehicle.
3. Kalman filter 4. Linear quadratic Gaussian 5. Model predictive control

1. Introduction

The *Springer* uninhabited surface vehicle (USV) has been built in Plymouth University and it continues to be further developed by the Marine and Industrial Dynamic Analysis Research Group. The USV being designed primarily for undertaking pollutant tracking, and environmental and hydrographical surveys in rivers, reservoirs, inland waterways and coastal waters, particularly where shallow waters prevail. In order for the vehicle to have such a multi-role capability, *Springer* requires robust, reliable and accurate NGC systems.

In previous work with the *Springer*, data from digital compasses are combined using various data-fusion architectures based on KFs (Xu, 2007). The use of redundant data (by using three separate compasses simultaneously) allows for the construction of fault-tolerant navigation systems. Another example is the USV *Charlie* that is equipped solely with a GPS and a magnetic compass which uses an extended KF (Caccia et al., 2008).

In this report the design of two autopilots are gauged against each other. For the NGC systems, common navigation and guidance subsystems are utilized in their designs. The navigation subsystem is based on a Kalman filter (KF) and the guidance subsystem on a waypoint line of sight (LOS) scheme. The control subsystems are designed using model predictive control (MPC) and linear quadratic Gaussian (LQG) controller. The performances of these controllers are assessed by way point following missions under the presence of external disturbances.

2. The *Springer* uninhabited surface vehicle.

2.1 Hardware

The details of the *Springer's* hardware are published in Sutton et al (2011). However, for the sake of completeness an outline is presented here. The *Springer* USV was designed as a medium waterplane twin hull vessel which is versatile in terms of mission profile and payload. It is approximately 4m long and 2.3m wide with a displacement of 0.6 tonnes. Each hull is divided into three watertight compartments. The NGC system is carried in watertight Peli cases and secured in a bay area between the crossbeams. The batteries which are used to provide the power for the propulsion system and on-board electronics are carried within the hulls, accessed by a watertight hatch. A mast has also been installed to carry the GPS and wireless antennas. The wireless antenna is used as a means of communication between the vessel and its user and is intended to be utilized for remote monitoring purpose, intervention in the case of erratic behaviour and to alter the mission parameters. The *Springer* is shown in Figure 1.

Figure 1. The *Springer* uninhabited surface vehicle

The *Springer* propulsion system consists of two propellers powered by a set of 24V 74lbs (334N) Minn Kota Riptide transom mounted saltwater trolling motors. As will be seen in subsection 2.2, steering of the vessel is based on the differential propeller revolution rates.

The TCM2, HMR3000 and KVH-C100 are the three different types of electronic compasses installed in the *Springer*. All of the compasses can output NMEA 0183 standard sentences with special sentence head and checksum. As all of these compasses are very sensitive, they were mounted as far as possible from any source of magnetic field and from ferrous metal objects. In addition, each compass was individually housed in a small waterproof case to provided further isolation and insulation.

2.2 Modelling the yaw dynamics

System Identification (SI) techniques have been applied to obtain the *Springer* model. For this, several trials were carried out where the vessel was driven for some calculated manoeuvres and data recorded at Roadford Reservoir, Devon, UK.

The vehicle has a differential steering mechanism and hence requires two inputs to adjust its course. This can be simply modelled as a two input, single output system in the form depicted in Figure 2.

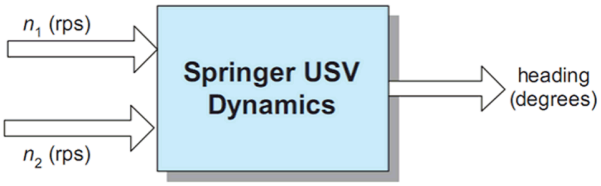

Figure 2. Block diagram representation of a two-input USV

In the above Figure 2, n_1 and n_2 represent the two propeller thrusts in revolutions per minute (rpm). Clearly, straight line manoeuvres require both the thrusters running at the same speed whereas the differential thrust is zero in this case. In order to linearise the model at an operating point, it is assumed that the vehicle is running at a constant speed of 3 knots. This corresponds to both thrusters running at 900 rpm. To clarify this further, let n_c and n_d represents the common mode and differential mode thruster velocities defined to be

$$n_c = \frac{n_1 + n_2}{2} \tag{1}$$

$$n_d = \frac{n_1 - n_2}{2} \tag{2}$$

In order to maintain the velocity of the vessel, n_c must remain constant at all times. The differential mode input, however, oscillates about zero depending on the direction of the manoeuvre. For data acquisition, several inputs including a pseudo random binary sequence (prbs) was applied to the thrusters and the heading response was recorded. SI was then applied to the acquired data set and a dynamic model of the vehicle is obtained in the following form.

$$\boldsymbol{x}(k+1) = \mathbf{A}\,\boldsymbol{x}(k) + \mathbf{B}\,u(k) \tag{3}$$

$$y(k) = \mathbf{C}\,\boldsymbol{x}(k) \tag{4}$$

where

$$\mathbf{A} = \begin{bmatrix} 1.002 & 0 \\ 0 & 0.9945 \end{bmatrix},\ \mathbf{B} = \begin{bmatrix} 6.354 \\ -4.699 \end{bmatrix} \times 10^{-6},$$
$$\mathbf{C} = \begin{bmatrix} 34.13 & 15.11 \end{bmatrix} \tag{5}$$

with a sampling time of 1s, where $u(k)$ represents the differential thrust input in rpm and $y(k)$ the heading angle in radians (Naeem et al, 2008).

3. Navigation, guidance and control system

A generalised integrated NGC system for the *Springer* USV is represented by the following block diagram as in figure 3.

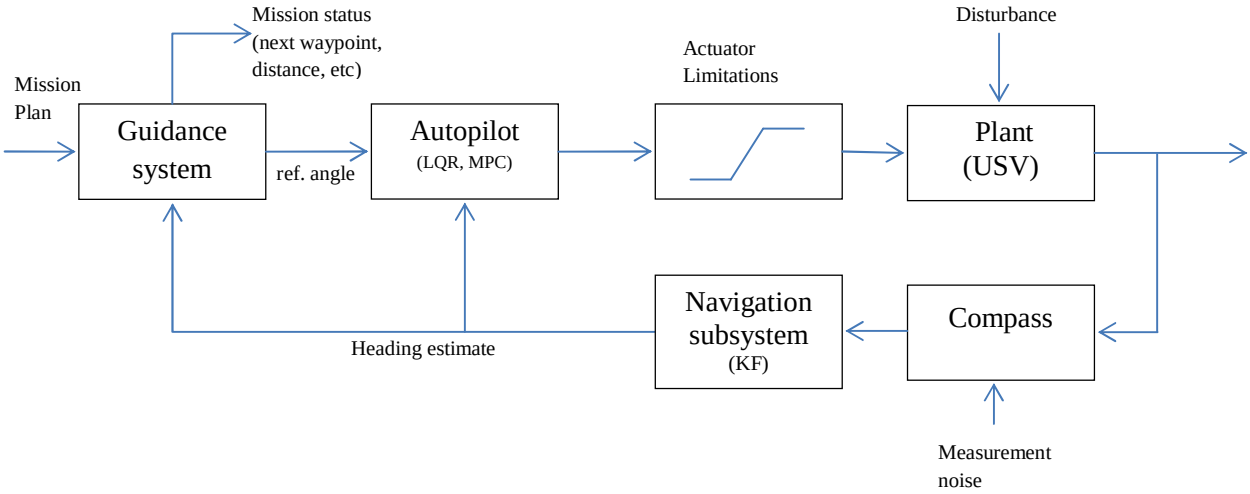

Figure 3. Block diagram of the integrated NGC system and USV model.

The mission plan consists of the set of predefined waypoints through which it is desired for the vessel to navigate. The particular mission plan used herein consists of seven waypoints forming a closed circuit is illustrated in the following Figure 4.

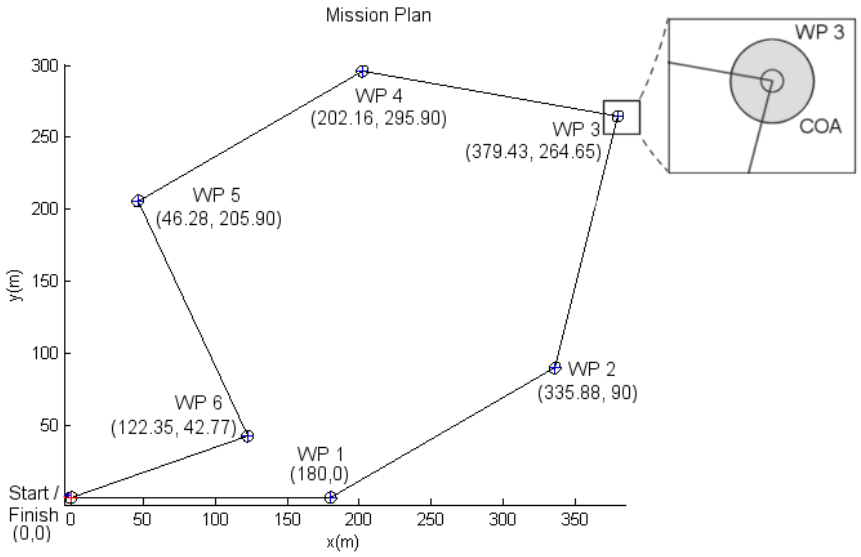

Figure 4. Mission plan: waypoint coordinates.

Based on the mission plan, the guidance system (described in detail in Section 5) keeps track of the mission status (previous and next waypoints, distance travelled and remaining, etc), generating the desired reference angle, or angle of the straight line connecting the vessel's current estimated position to the next waypoint. In turn, based on the desired reference angle and the current estimated heading of the vessel (or estimated state vector of the USV model in the case of LQG control), the autopilot, or controller, generates the most adequate control signal, or differential thrust of the motors (recall that steering is controlled via the differential mode thruster velocity, n_d). The autopilot herein is concerned only with heading control, since, as was previously stated, the common mode thruster velocity n_c is maintained constant throughout.

The heading estimate of the vessel is provided by the navigation system. The position of the vessel is calculated via dead-reckoning since the forward speed of the vessel is known. These calculations are described in more detail in the following sections.

It should be mentioned that in this simulation study, the actual vessel is substituted by its mathematical model. The yaw dynamics of the actual USV is simulated using the second order state-space model described by (8) and (9), where an additional term, $\boldsymbol{\omega}(k)$, has been added to equation (8) to represent a random input disturbance, and is generated from a Normal distribution with zero mean and covariance $diag\{1,1\}\times 10^{-14}$. On the other hand, the forward speed of the USV is assumed to be a constant 3 knots (1.5433m/s). The next section details the navigation subsystem on board.

4. Navigation

The navigation system of the vessel provides the heading estimate. The heading estimator is based on Kalman filtering which combines predictions from a dynamic model of the compass with actual compass measurements (simulations of these for this study).

Kalman filter

For linear systems described via state-space equations that incorporate stochastic uncertainty (Motwani et al, 2012) in the state and output equations, that is, systems that may be described by

$$\boldsymbol{x}(k+1) = \mathbf{A}\,\boldsymbol{x}(k) + \mathbf{B}\,u(k) + \boldsymbol{\omega}(k) \tag{6}$$

and

$$y(k) = \mathbf{C}\,\boldsymbol{x}(k) + \upsilon(k) \tag{7}$$

it is well established that the KF provides statistically optimal estimates of the state vector (a detailed derivation can be found in Chui and Chen (2008)).

In this report, the model of the TCM2 compass obtained by Xu (2007) is used and is described as

$$\begin{aligned} &\mathbf{A} = \begin{bmatrix} 0.2796 & 0.6971 \\ 1 & 0 \end{bmatrix}, \quad \mathbf{B} = \begin{bmatrix} 0.4364 \\ 0 \end{bmatrix} \\ &\mathbf{C} = \mathrm{K}\begin{bmatrix} 1 & 0 \end{bmatrix} \\ &cov(\boldsymbol{\omega}) = diag\{1,1\}, \quad \sqrt{var(\upsilon)} = 2^\circ \end{aligned} \tag{8}$$

The sampling period was 0.025s. The input to the model is the actual heading of the vessel, in degrees, and the output is the compass measurement, also in degrees, whereby it can be assumed that the constant K is such that the steady-state gain of the model is unity (resulting in K = 0.05339). The KF based on this model together with measurement simulations provides an estimate of the state vector which forms part of the LQG feedback loop, as well as an estimate of the heading angle, used in the feedback loop of the MPC autopilot and by the guidance system to generate the desired heading angle. The subsequent sections detail the LQG and MPC autopilots used in this study.

5. Guidance subsystem

Different guidance strategies used in marine environments to guide the vehicles are further illustrated in Annamalai (2012). The most popular guidance strategy is waypoint LOS strategy and is utilised in this study. It is briefly illustrated in the following subsection 5.1.

5.1 Waypoint line of sight guidance

Based on the current estimated position of the USV and the coordinates of the next waypoint to be reached, the desired or reference heading angle based on LOS is calculated as follows:

$$r(k) = tan^{-1}\left[\frac{y_d(k)-y(k)}{x_d(k)-x(k)}\right] \tag{9}$$

where (x,y) is the current location of the vessel and (x_d,y_d) the target coordinates. In practice, because the inverse of the tangent is restricted to (-90°,90°), the four quadrant inverse tangent, $arctan2(y_d(k)-y(k), x_d(k)-x(k))$, which takes into account the signs of both arguments, is used instead. Care is also taken to ensure that the vessel is directed to turn toward the updated reference angle from its present heading in the direction of rotation that requires the lesser change in angle with respect to its present heading angle, since two possibilities always exist.

The guidance system keeps track of the mission status, which includes a log of the waypoints reached or missed and the current target waypoint, as well as the total distance travelled, deviation from the ideal trajectory, and controller energy consumed. These are updated every sampling instant given the updated estimates of the position and heading of the USV.

In order to decide whether a waypoint has been reached or not, the guidance system considers a circle of acceptance (COA) around each of these (Figure 5). A COA is needed since the marine environment is continuously moving with some degree of randomness, making it unfeasible in practice to target a single point precisely. Healey and Lienard (1993) suggest that the radius of the COA should be at least twice the length of the vehicle. However, their concern was to do with underwater vehicles. Since surface vessels benefit from GPS, a radius equal to the length of the vessel is deemed sufficient herein. For Springer the length is approximately 4m, thus this is the radius assigned to the COA. At each sampling instant, the guidance system calculates the distance left to the next waypoint according to

$$\rho = \sqrt{[x_d(k)-x(t)]^2 + [y_d(k)-y(t)]^2} \leq \rho_0 \tag{10}$$

where ρ_0 is the radius of the COA. When this condition is met then it is concluded that the waypoint is reached, and the guidance system directs the vessel to the following waypoint. As a practical consideration during implementation, note that the vessel's coordinates may not be within the COA at the sampling instants of time (simulation instants), though it may have entered and left it in between sampling instants. The criterion used here is that if the straight line between two position estimates penetrates the COA even though the two estimates do not, then it is considered that the waypoint in question has been reached.

However, the vessel might pass by the vicinity of a waypoint without entering the COA. This condition is determined by checking the derivative $d\rho/dt$, which when switches from negative to positive, indicates that the vessel has missed the waypoint. In this case, the guidance system also directs the vessel toward the next waypoint.

The vessel normally follows a path different from the ideal one. Several performance indices are used to assess the trajectories followed, which the guidance system computes at each time step and keeps track of. The deviation from the ideal trajectory can be measured as

$$rd(k) = \sqrt{r^2(k) + r'^2(k) - 2r(k)r'(k)\cos\alpha} \tag{11}$$

where $r(k)$ is the distance to the next waypoint from the position of the vehicle were it on the ideal path, and $r'(k)$ the distance to the next waypoint from the actual position of the vessel, α being the angle between the two vectors, as shown in Figure 5.

The average controller energy $\overline{CE_u}$ is defined as

$$\overline{CE_u} = \frac{\sum_{k=0}^{N} [u_c(k)/60]^2}{N} \tag{12}$$

where N is the total number of time steps and u_c the controller effort at time k in *rpm*.

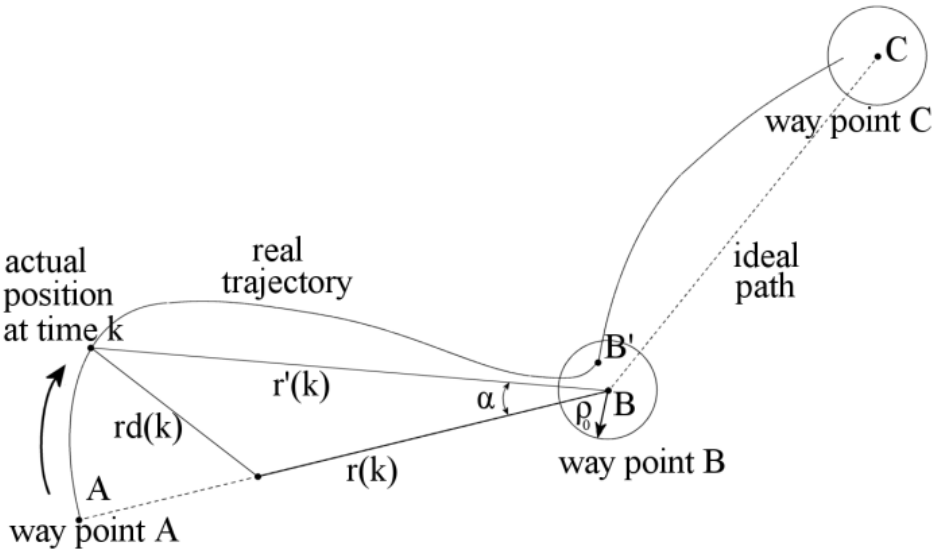

Figure 5. Deviation at time *k*

6. Linear quadratic Gaussian autopilot

In a traditional autopilot design, an LQG controller is generally selected which consists of a linear combination of a linear quadratic state feedback regulator (LQR) and a KF. The LQG controller is inherently multivariable therefore modification to a multi-input multi-output model is rather straightforward. To construct the autopilot, an LQR problem is solved which assumes that all states are available for feedback. However, this is not always true because either there is no available sensor to measure that state or the measurement is very noisy. A KF can be designed to estimate the unmeasured states. The LQR and KF are developed independently and then combined to form an LQG controller, a fact known as the separation principle. A block diagram of the autopilot is depicted in Figure 6 showing the individual components of the LQG.

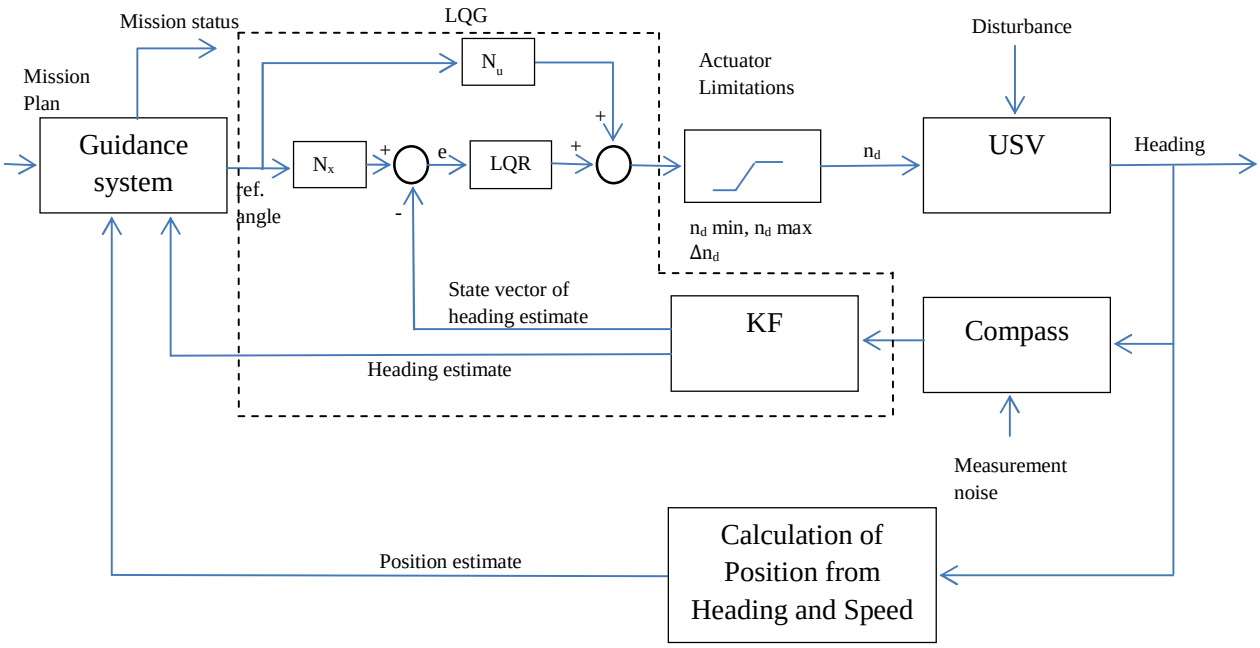

Figure 6. NGC system with LQG controller

The LQG controller requires a state space model of the system in the form specified in (3) and (4). In this case, the matrices A, B, C, and D are defined in (5) for the *Springer* vehicle. A unique closed form solution of the LQG control law is defined as

$$u(k) = \underset{\substack{L \\ Q \\ R}}{K} (x_r(k) - \hat{x}(k)) \quad (13)$$

where $\hat{x}$ is the KF estimate of the state vector of the *Springer* state-space model. Furthermore, concerning the choice of parameters Q and R. $Q = C^T C$, R being a scalar so that the cost function takes the following form

$$J = \sum \|y\|^2 + R \sum \|u\|^2 \quad (14)$$

7. Model predictive control autopilot

The concepts and techniques of MPC have been developed over the past three decades (Annamalai, 2012) and are shown to be popular in many sectors such as the process and automotive industries, and in academia as illustrated in the text of Maciejowski (2002), Rawlings and Mayne (2009), Wang (2009) and Allgower et al (2010). In addition, the marine control system design fraternity have also embraced this approach since it offers the advantage of being capable of enforcing various types of constraints on the plant process as exemplified by Naeem et al (2005), Perez (2005), Oh and Sun (2010), Liu et al (2011), and Li and Sun (2012).

In general, the plant output is predicted by using a model of the plant to be controlled. Any model that describes the relationship between the input and the output of the plant can be used. Further if the plant is subject to disturbances, a disturbance or noise model can be added to the plant model. In order to define how well the predicted process output tracks the reference trajectory, a criterion function is used. Typically the criterion is the difference between the predicted process output and the desired reference trajectory. A simple criterion function is,

$$J = \sum_{i=1}^{H_p} [\hat{y}(k+i) - w(k+i)]^2 \tag{15}$$

where $\hat{y}$ is the predicted process output, w is the reference trajectory, and H_p is the prediction horizon or output horizon. The general structure of an MPC is shown in the following Figure 7(a).

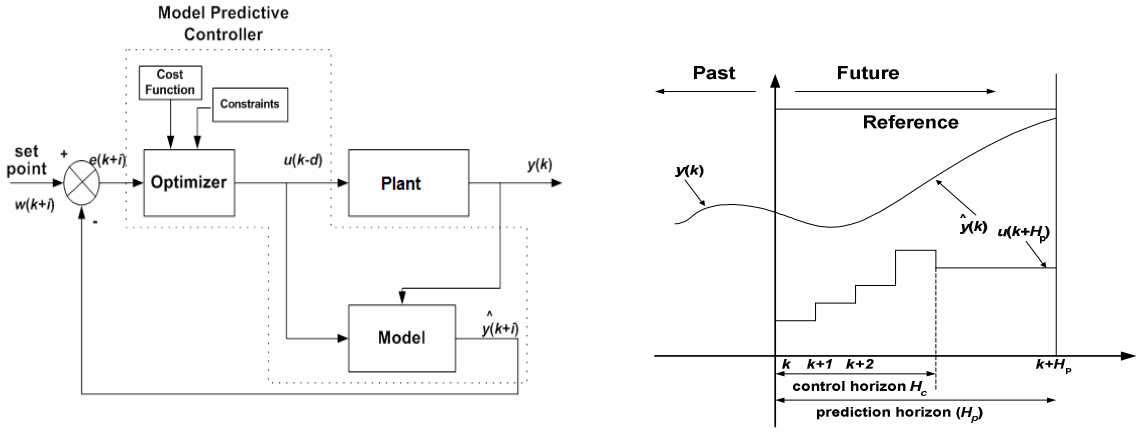

(a) General structure of MPC (b) General strategy of MPC

Figure 7: MPC (a) general structure; (b) general strategy

The optimal controller output sequence $\boldsymbol{u_{opt}}$ over the prediction horizon is obtained by minimisation of J with respect to u. As a result the future tracking error is minimised. If there is no model mismatch i.e. the model is identical to the plant and there are no disturbances and constraints, the process will track the reference trajectory exactly on the sampling instants.

The MPC algorithm consists of the following three steps.

Step 1. Use a model explicitly to predict the process output along a future time horizon (Prediction Horizon).

Step 2. Calculate a control sequence along a future time horizon (Control Horizon, H_c), to optimize a performance index.

Step 3. Employ a receding horizon strategy so that at each instant the horizon is moved towards the future, which involves the application of the first control signal of the sequence calculated at each step. The strategy is illustrated as shown in Figure 7(b).

In the above Figure 7(b), the predicted output and the corresponding optimum input over a horizon H_p, where $u(k)$ is the optimum input, $\hat{y}(k)$ is the predicted output, and $y(k)$, process output.

The controller is not fixed and is designed at every sampling instant based on actual sensor measurements so disturbances can easily be dealt with as compared to fixed gain controllers.

In this study, the plant output $y(k)$ is obtained from the KF estimate and the cost function optimised is of the following form,

$$J = \sum_{i=1}^{H_p} e(k+i)^T Q\, e(k+i) + \sum_{i=1}^{H_c} \Delta u(k+i)^T\, R\, \Delta u(k+i) + \sum_{i=1}^{H_p} u(k+i)^T\, S\, u(k+i) \tag{16}$$

subject to,

$$u^l \leq u(k+i) \leq u^u$$
$$\Delta u^l \leq \Delta u(k+i) \leq \Delta u^u$$

where the superscripts l and u represent the lower and the upper bounds respectively. Q is the weight on the prediction error,

$$e(k) = \hat{y}(k) - w(k)$$

R and S are the weights on the change in the input Δu and magnitude of the input u respectively. More details can be found in Naeem et al. (2005).

The values of the weights used in this study are as detailed in the following table 1.

Weights	**Values**
Q	1
R	0.1
S	0

Table 1: Value of weights used in MPC cost function

The integration of the NGC system is detailed in the following figure 8.

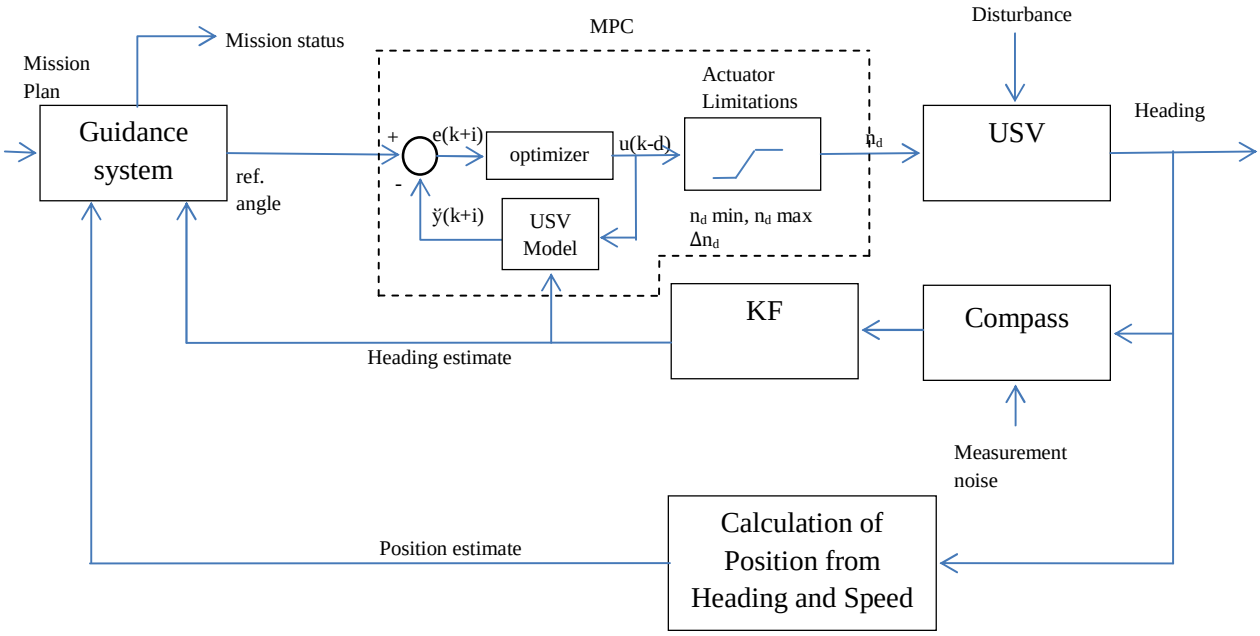

Figure 8. NGC system with MPC controller

8. Simulation and results.

The performance of the LQG and MPC autopilots are compared in this section. A disturbance of 10% current acting in a northerly direction is added throughout the simulation to recreate realistic environments.

The position of the vessel at each time step is calculated from the previous using dead reckoning, given that the forward speed of the vessel (relative to the water surface) is constant and known. Added to this, a constant disturbance consisting of an added velocity of 10% of the forward speed of the vessel, acting in a northerly direction, was added to consider the effect of surface currents (Figure 9). If x(k) and y(k) represent the position of the vessel at time k, then the position at the next sample time is calculated as follows:

$$x(k+1) = x(k) + v\,T_s\cos(\theta) \tag{17}$$

$$y(k+1) = y(k) + v\,T_s\sin(\theta) + 0.10\,v\,T_s \tag{18}$$

where v is the constant forward speed of the vessel (three knots), T_s the sampling interval 1s, θ the actual heading angle of the vessel at time k, and the disturbance of 0.10 v Ts has been added to the y component.

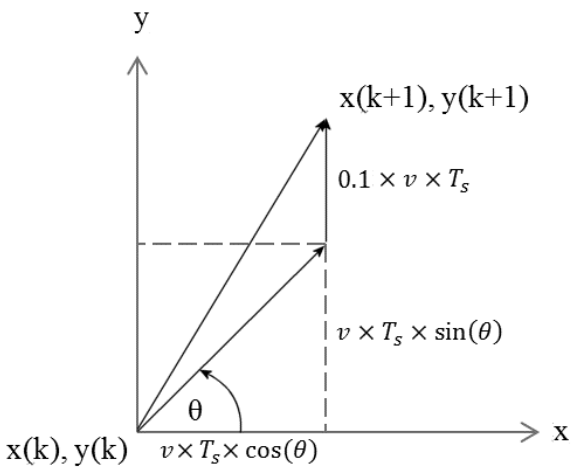

Figure 9. Effect of disturbance on calculation of position of the USV

The following figures 10 and 11, show typical simulations results for each of the two autopilots. Figures 10(a) and 11(a) depict the position of the USV, both the actual position and the one estimated by the filtered GPS data, as well as information provided by the guidance system. Figures 10(b) and 11(b) show the output of the respective controllers, and Figures 10(c) and

11(c) show the step changes of the control signal (Δn_d). It can be seen how these are limited due to the actuator saturation limits considered. These have been imposed as

$$|n_d| < 300rpm \text{ and } |\Delta n_d| < 20rpm$$

a limitation both on the maximum absolute value and the maximum step changes of the motors.

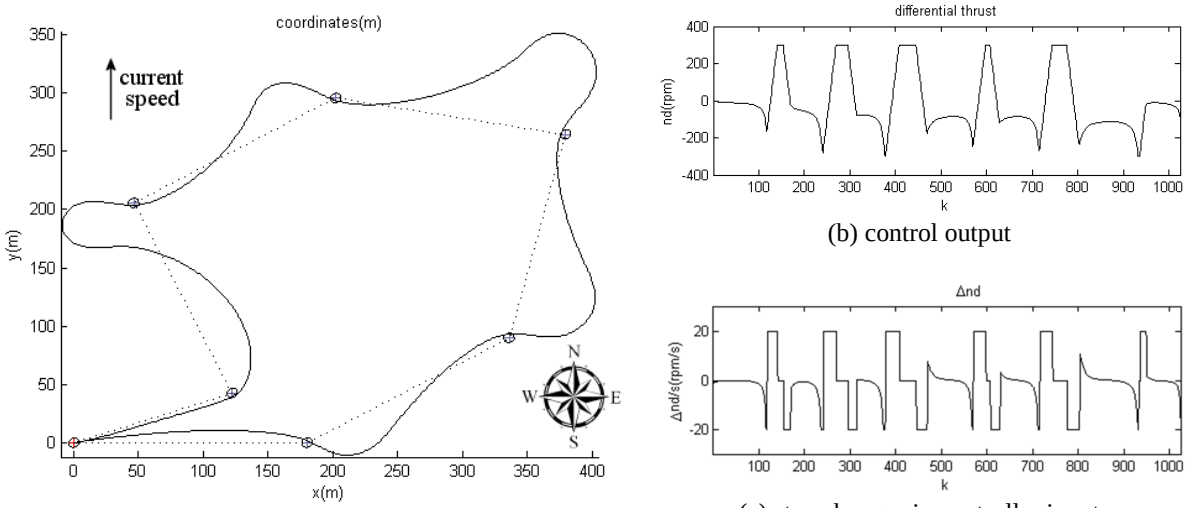

(a) trajectory (b) control output (c) step changes in controller input

Fig 10 (a) Way point tracking by LQG autopilot (b) Differential thrust (c) Step changes in controller input

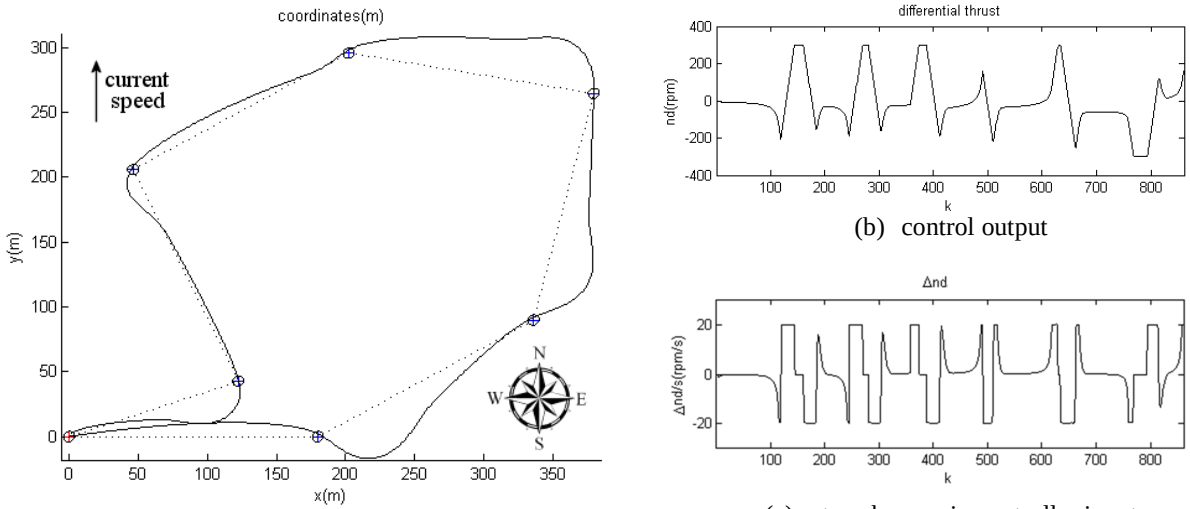

(a) trajectory (b) control output (c) step changes in controller input

Fig 11 (a) Way point tracking by MPC autopilot (b) Differential thrust (c) Step changes in controller input

The performance indices measured to compare the autopilots were: number of waypoints reached (out of 7), total distance travelled, average deviation and average controller energy. The results are summarised in the following table 2.

Parameters	**LQG autopilot in NGC**	**MPC autopilot in NGC**
Number of waypoints reached	7	7
Total distance travelled	1552.92 m	1305.39 m
Average deviation	45.17 m	19.09 m
Average energy	6.581 rps^2	4.536 rps^2

Table 2: Comparison of Autopilots

The waypoint tracking indicates that the trajectory followed by MPC autopilot is much smoother and better than that of the LQG. Both the MPC controller and the LQG reach all the waypoints under the given circumstances. The MPC autopilot travels less distance than the LQG to cover the same 7 waypoints in this study. Henceforth the MPC has a correspondingly less average deviation and average controller energy. Moreover, the controller action generated by the LQG controller exhibits more sudden changes in comparison to the MPC controller action. Hence overall, the results demonstrate that the MPC autopilot clearly outperforms the LQG controller.

9. Conclusion

The LQG and MPC autopilots are compared for inclusion in an integrated navigation, guidance and control system for an USV. Various parameters of the autopilots performance were analysed and the results were discussed in the previous section. Kalman filtering was used to provide the navigation estimates and the line of sight guidance system was utilised to generate the reference heading to be achieved by the control subsystems. With regard to the autopilots, the MPC clearly outperforms the LQG with respect to the performance parameter measures used. Hence MPC is recommended as a suitable autopilot for USVs. This study further demonstrates that MPC can cope with fast changing dynamics of the plant and can perform well when integrated with the other subsystems in USVs.

References

Allgower, F., Glielmo, L., Guardiola, C., and Kolmanovsky, I., (2010). *Automotive model predictive control.* Springer-Verlag, Berlin.

Annamalai, A.S.K., (2012). A review of model predictive control and closed loop system identification for design of an autopilot for uninhabited surface vehicles. MIDAS Technical Report: MIDAS.SMSE.2012.TR.005

Caccia, M., Bibuli, M., Bono, R., and Bruzzone, G., (2008). Basic navigation, guidance and control of an unmanned surface vehicle. *Journal of Autonomous Robots*, Vol 25, No 4, pp.349-365.

Chui, C.K. and Chen, G. (2008). *Kalman Filtering with Real-Time Applications*, 4th ed. Springer, New York.

Healey, A. J., and Lienard, D., (1993). Multivariable sliding model control for autonomous diving and steering of unmanned underwater vehicles. IEEE Journal of Oceanic Engineering, Vol 18, No 3, pp.327-339.

Li, Z., and Sun, J., (2012). Disturbance compensating model predictive control with application to ship heading control. *IEEE Trans on Control Systems Technology*, Vol 20, No 1, January, pp.257-265.

Liu, J., Allen, R., and Yi, H., (2011).Ship motion stabilizing control using a combination of model predictive control and an adaptive input disturbance predictor. *Proc IMechE Part I: Journal of Systems and Control Engineering* , Vol 225, No 5, August, pp.591-602.

Maciejowski, J.M., (2002). *Predictive control with constraints.* Prentice Hall Inc, London.

Motwani, A., Sharma, S.K., Sutton, R., Culverhouse, P., (2012). Interval kalman filtering in navigation system design for an uninhabited surface vehicle. Journal of Navigation (submitted for publication).

Naeem, W., Sutton, R., Chudley J., Dalgleish F.R., and Tetlow, S., (2005). An online genetic algorithm based model predictive control autopilot design with experimental verification. *International Journal of Control*, Vol 78, No 14/20, September, pp. 1076-1090.

Naeem W, Xu T, Sutton R and Tiano A. 2008. The design of a navigation, guidance, and control system for an unmanned surface vehicle for environmental monitoring. Proc Instn Mech Engrs Part M: Journal of Engineering for the Maritime Environment, Vol 222, No M2, 67–80

Oh, S.R., and Sun, J., (2010). Path following of under actuated marine surface vessels using line-of-sight based model predictive control. Ocean Engineering, Vol 37, No 2-3, pp.289-295.

Perez, T., (2005). Ship motion: Course keeping and roll stabilisation using rudder and fins. Springer-Verlag, London.

Rawlings, J.B., and Mayne, D.Q., (2009). Model predictive control: Theory and design. Nob Hill Publishing, Madison.

Sutton, R., Sharma, S., and Xu, T., (2011). *Adaptive navigation systems for an unmanned surface vehicle*, Proc IMarEST - Part A: Journal of Marine Engineering and Technology, Vol 10, No 3, September, pp.3-20.

Wang, L., (2009). *Model predictive control system design and implementation using MATLAB*. Springer-Verlag, Berlin.

Xu, T., (2007). *An intelligent navigation system for an unmanned surface vehicle*. PhD thesis, Plymouth University, UK.

Nomenclature / List of Acronyms

COA	Circle of acceptance
GPS	Global Positioning System
KF	Kalman Filter
LOS	Line of Sight
LQG	Linear Quadratic Gaussian
MPC	Model Predictive Control
NGC	Navigation, Guidance, and Control
PRBS	Pseudo Random Binary Sequence
Q	Process Noise Covariance
R	Measurement Noise Covariance
SI	System Identification
USV	Uninhabited Surface Vehicle